

Abundance analysis of giant H II regions in M51

Angeles I. Díaz,¹ Elena Terlevich,² José M. Vilchez,³ Bernard E. J. Pagel⁴ and Michael G. Edmunds⁵

¹Departamento de Física Teórica, C-XI, Universidad Autónoma de Madrid, 28049 Madrid, Spain

²Royal Greenwich Observatory, Madingley Rd, Cambridge CB3 0EZ

³Instituto de Astrofísica de Canarias, 38200 La Laguna, Tenerife, Spain

⁴NORDITA, Blegdamsvej 17, DK-2100 København Ø, Denmark

⁵Department of Physics, University of Wales College of Cardiff, PO Box 913, Cardiff CF1 3TH

Accepted 1991 July 3. Received 1991 June 17; in original form 1991 April 5

SUMMARY

We present spectrophotometric observations in the optical and near infrared of six giant H II regions in the high metallicity spiral galaxy M51. Five of the regions are located in the spiral arms and the sixth one is very close to the nucleus. These observations and the application of adequate photo-ionization models allow the determination of the functional parameters of the regions: ionization parameter, effective temperature of the ionizing radiation and metallicity. The results of this work confirm previously found trends of decreasing ionization parameter and radiation hardness with increasing metallicity. N/O and S/O ratios are in general higher and lower than solar respectively. The first trend is expected from the view point of stellar nucleosynthesis and chemical evolution theories. However, the existence of a lower S/O ratio in regions of high metallicity, if confirmed as real, needs to be accounted for.

1 INTRODUCTION

Giant H II regions are easily observable on the discs of nearly face-on spiral galaxies. These observations constitute the most currently used means of deriving information about the chemical composition of the interstellar medium of external galaxies. The abundance variations of different elements are important constraints for chemical evolution models and the detailed study of the behaviour of element ratios constitutes a test of nucleosynthesis and stellar evolution theories (see e.g. Díaz 1989 and references therein).

These studies have been devoted preferentially to regions of relatively low metal content. The high excitation of these regions allows the detection of the weak temperature-sensitive lines required for reliable abundance determinations (e.g. [O III] $\lambda 4363$ Å, [N II] $\lambda 5755$ Å etc.). In the absence of these lines, empirical calibrations of strong emission line intensities with electron temperatures or oxygen abundances can be used (Pagel *et al.* 1979; Alloin *et al.* 1979) but uncertainties can be large for the high metallicity end of the relation which has to be calibrated on the basis of theoretical models [Edmunds & Pagel 1984; McCall, Rybski & Shields 1985 (hereafter MRS); Dopita & Evans 1986]. This makes low-excitation regions of correspondingly higher metallicity more difficult to study.

Recently Vilchez & Pagel (1988), following earlier work by Shields & Searle (1978) and Mathis (1982, 1985), have

developed an alternative method consisting of the simultaneous fitting of the empirical parameter for abundance proposed by Pagel *et al.* (1979) and a ‘radiation softness’ parameter characterizing the ionizing spectrum, to an appropriate grid of theoretical models (e.g. Stasińska 1982). This method requires an extensive wavelength coverage including the near infrared [S III] lines ($\lambda\lambda 9069, 9532$ Å) and has been applied by Díaz *et al.* (1987) and Vilchez *et al.* (1988) to determine abundances and some physical properties of seven giant H II regions in the nearby spiral M33, among them the low excitation region CC93 located very close to the galaxy nucleus.

We have extended this study to regions of low excitation by analysing six of the giant H II regions of M51 using photo-ionization models computed with the most recent version of the CLOUDY code (Ferland 1990). The observations required for this analysis are described in Section 2 of this paper; the results are presented in Section 3 and discussed in Sections 4 and 5. Finally, Section 6 summarizes the main conclusions of this work.

2 OBSERVATIONS AND REDUCTIONS

M51 is a nearly face-on Sc galaxy with a well-defined spiral structure. It is also classified as ‘peculiar’, its peculiarity being attributed to the presence of a small companion with which it is interacting. Its nuclear region has been extensively studied

(Rose & Searle 1982; Rose & Cecil 1983) showing an unusually high [N II]/H α ratio. The nuclear spectrum corresponds to the class referred to as LINER (Low Ionization Nuclear Emission-line Region).

Five of the H II regions observed were selected from the study of Carranza, Crillon & Monnet (1969, hereafter CCM) and are marked on the H α photograph taken with the Isaac Newton Telescope in its previous location at Herstmonceux (Plate 1). Their size and physical properties place them in the category of giant H II regions similar to NGC 604 in M33 and 30 Dor in the LMC (van der Hulst *et al.* 1988).

A sixth region was identified on the long slit spectrum taken at position angle 340° (see next section). This region, located at 30 arcsec from the nucleus is labelled X in Table 1 and subsequent references.

The observations consist of long-slit spectrophotometry using two different detectors: IPCS for the blue spectral region from λ 3600–7500 Å and CCD for the red (λ 6200–7500 Å) and the near infrared (λ 8500–9800 Å). The large overlap between IPCS and CCD spectra allows an adequate merging of both.

The observations were made on 1985 March 20–22 (CCD spectra) and 1987 February 21–23 (IPCS) with the Isaac Newton Telescope of the ING in the Observatorio del Roque de los Muchachos (La Palma), the RGO 235-mm camera and the Intermediate Dispersion Spectrograph (IDS). The gratings used with each of the two detectors (300 and 400 grooves mm⁻¹ for IPCS and CCD respectively, giving dispersions of 137 Å mm⁻¹ and 104 Å mm⁻¹) provide a uniform element resolution of about 2 Å per pixel. With the slit width used (1 arcsec for the IPCS data and 1.50 arcsec for the CCD ones) the corresponding spectral resolutions are 4.7 and 5.2 Å. The spatial resolution is 0.82 arcsec for the IPCS and 0.7 arcsec for the CCD. The seeing was between 1.2 and 1.5 arcsec. A journal of observations is given in Table 1.

The reduction of the data was performed at the RGO and the IAC using STARLINK software. The detailed procedure is described in Díaz *et al.* (1987). The wavelength calibration was accurate to 1 Å in all cases. The H α spatial profiles corresponding to the three slit positions used are shown in Fig. 1. Marked on the profiles are each of the extractions for the regions observed. Suitable portions of the sky for background subtraction were extracted from the outer parts of the slit, except for the IPCS observations of the H II region closest to the nucleus, X, for which a separate sky observation was made. The sky subtraction on all occasions seemed to be good.

CCD data are affected by atmospheric absorption (see Díaz, Pagel & Wilson 1985). The removal of this effect was

achieved dividing by the spectrum of a subdwarf star observed on the same night as the object. At any rate, the redshift of M51 seems to place the [S III] lines out of the narrow water vapour absorption lines as evidenced by the ratio derived for them which is very close to the theoretical one (see Section 3 and Table 2).

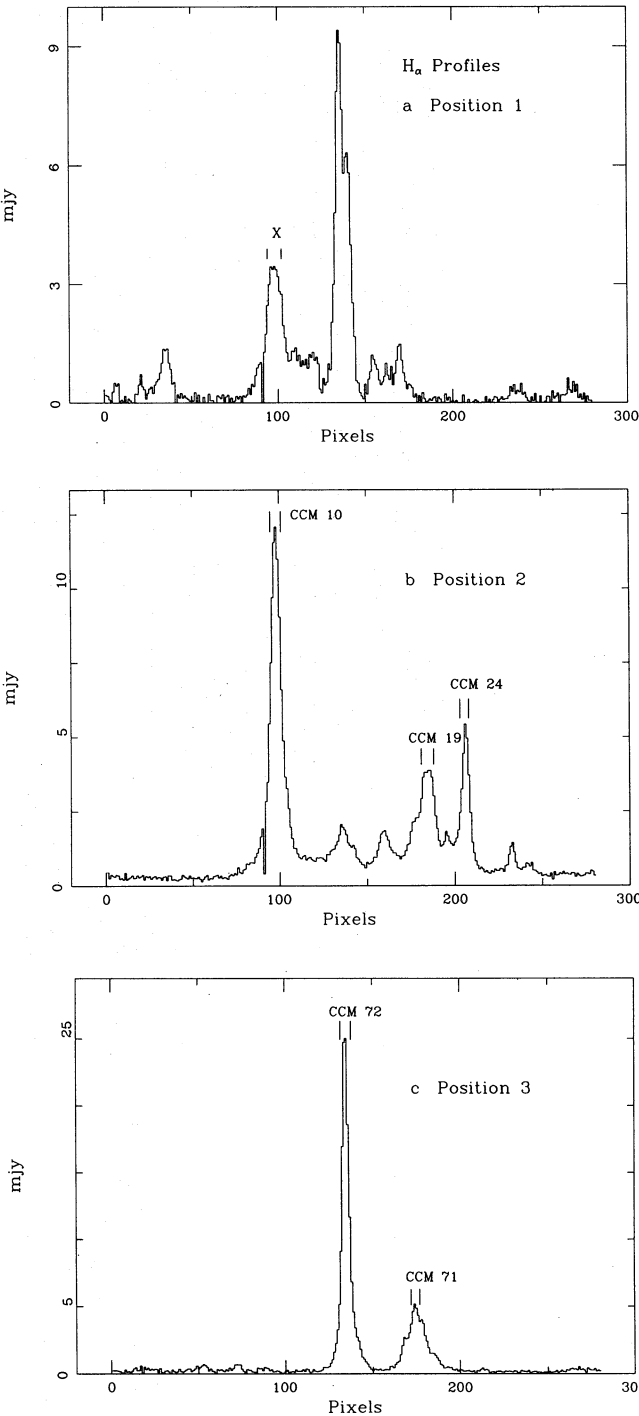


Figure 1. H α spatial profiles for the three slit positions used in the observations: (a) position including the nucleus and region X; (b) position including regions CCM10, CCM19 and CCM24; (c) position including regions CCM71 and CCM72.

Table 1. Journal of observations.

Region	Night	Detector	P.A.	Grating	$\Delta\lambda(\text{\AA})$	Exposure (s)
X	85 Mar 20/21	CCD	340	R400R	6200-7600	1000
X	85 Mar 20/21	CCD	340	R400R	7300-8700	1500
X	85 Mar 20/21	CCD	340	R400R	8400-9800	2000
X	87 Feb 21/22	IPCS	340	R300V	3500-7500	1500
71-72	85 Mar 20/21	CCD	340	R400R	6200-7600	1000
71-72	85 Mar 20/21	CCD	340	R400R	8400-9800	2000
71-72	85 Mar 20/21	CCD	340	R400R	8400-9800	1000
71-72	87 Feb 22/23	IPCS	340	R300V	3500-7500	1500
10-19-24	85 Mar 20/21	CCD	340	R400R	6200-7600	1000
10-19-24	85 Mar 20/21	CCD	340	R400R	8400-9800	2500
10-19-24	87 Feb 22/23	IPCS	340	R300V	3500-7500	1500

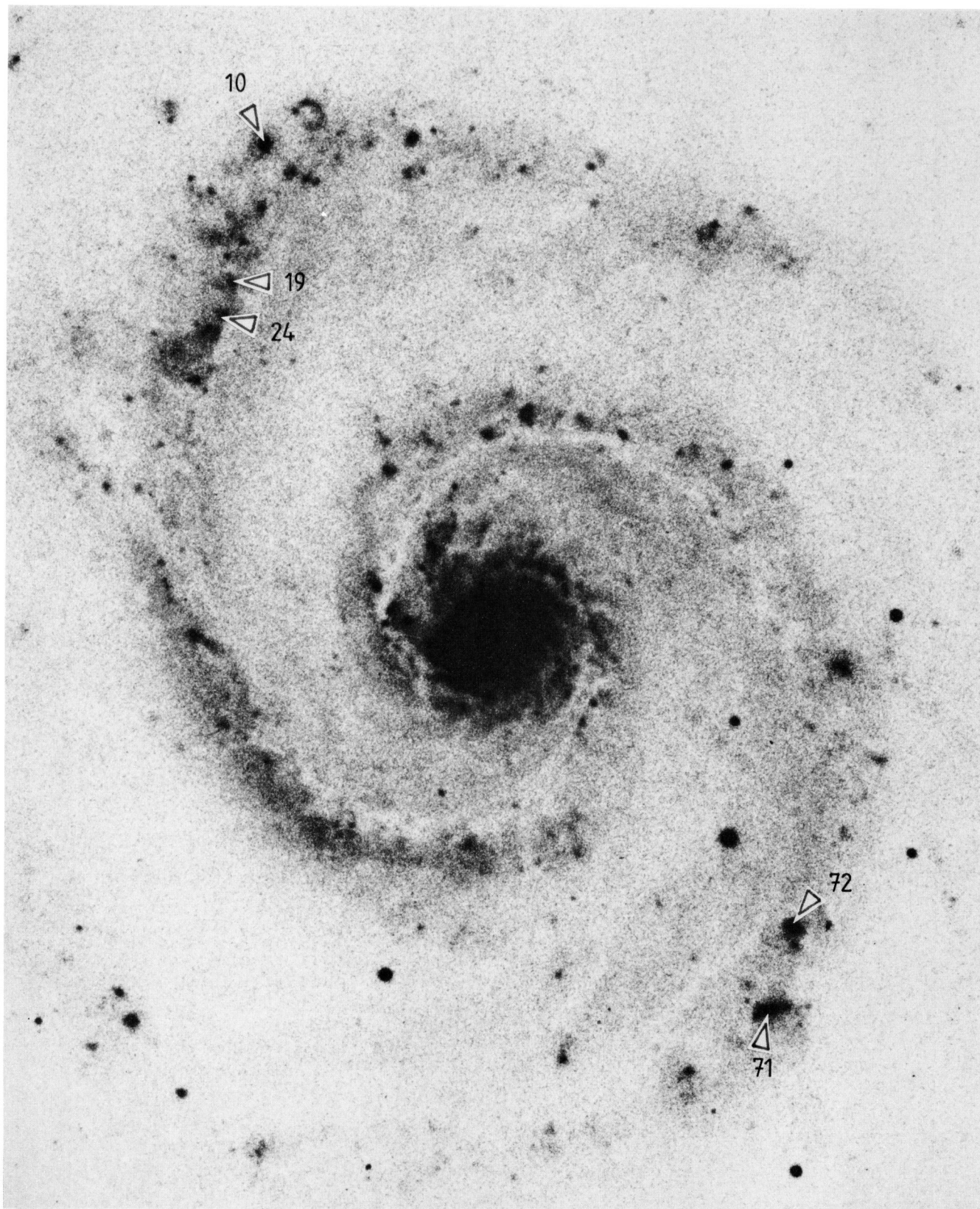


Plate 1. $H\alpha$ photograph of M51 taken with the INT in its previous location at Herstmonceux. The $H\text{ II}$ regions observed for this study are marked.

Table 2. Emission line fluxes.

Region			X	CCM 72	CCM 24	CCM 19	CCM 71	CCM 10
Line	$f(\lambda)$	$i(\lambda)$						
3727 [OII]	0.26		115 ± 12	61 ± 6	102 ± 5	≤ 28	46 ± 12	162 ± 12
4102 H δ	0.18	26	13 ± 4	25 ± 4	18:	≤ 10	25 ± 5	32 ± 3
4340 H γ	0.135	47	47 ± 4	46 ± 4	50 ± 3	43 ± 10	50 ± 5	59 ± 6
4861 H β	0.00	100	100 ± 5	100 ± 5	100 ± 4	100 ± 12	100 ± 6	100 ± 8
5007 [OIII]	-0.03		24 ± 10	5 ± 2	17 ± 10	≤ 14	< 7	20 ± 2
5876 HeI	-0.23		—	6 ± 2	—	—	12 ± 4	13 ± 1
6563 H α	-0.34	286	282 ± 21	286 ± 6	314 ± 32	289 ± 30	287 ± 29	300 ± 21
6584 [NII]	-0.34		68 ± 5	92 ± 2	108 ± 11	78 ± 8	86 ± 9	116 ± 8
6717 [SII]	-0.36		20 ± 3	20 ± 2	24 ± 2	23 ± 4	21 ± 3	23 ± 3
6731 [SII]	-0.36		13 ± 2	17 ± 2	18 ± 1	16 ± 2	14 ± 2	17 ± 3
8750 P12	-0.59	1.11	—	1.5 ± 0.6	—	—	—	—
8863 P11	-0.60	1.37	—	1.2 ± 0.6	—	—	—	—
9015 P10	-0.62	1.85	—	1.9 ± 0.6	1.4 ± 0.6	—	1.8 ± 0.8	1.6 ± 0.6
9069 [SIII]	-0.64		3:	14 ± 2	12 ± 5	1.9:	10 ± 1	10 ± 1.5
9229 P9	-0.64	2.55	—	2.3 ± 1.0	3 ± 1	—	1:	2.0 ± 0.3
9532 [SIII]	-0.65		8 ± 2	37 ± 6	21 ± 9	5:	31 ± 3	23 ± 3.5
9546 P8	-0.65		—	6 ± 1.0	6 ± 1.5	—	5 ± 1	3.8 ± 1.0
c(H β)			0.70	0.31	0.6:	0.16:	0.21	0.3:
F(H α)*			14.6	43.8	7.5	9.8	16.9	26.5
I(H β)*			15.0	24.5	6.0	4.3	8.1	14.0
EW(H β) (Å)			7	64	22	19	22	48

* 10^{-14} erg cm $^{-2}$ s $^{-1}$ $i(\lambda)$ are the expected values for the Balmer and Paschen lines normalized to H β = 100 (case B, Brocklehurst 1971).

3 RESULTS

3.1 Emission line fluxes

Reduced spectra are shown in Figs 2–4 for regions CCM72, CCM10 and X, each one corresponding to one of the slit positions, for the optical region (IPCS) and the near infrared (CCD); the most relevant emission lines are marked. Given the low excitation of the regions observed, the [O III] λ 5007 Å line is very weak; however, the near-infrared [S III] $\lambda\lambda$ 9067, 9532 Å lines are easily observable.

Emission line fluxes were measured in each spectrum integrating the flux under the line profile and over a fitted linear continuum. Errors for line fluxes were calculated following Poisson photon statistics including sky and continuum. Errors in continuum placement are estimated on the basis of repeated measurements.

The logarithmic extinction at H β was derived from the Balmer decrements H δ /H β , H γ /H β and H α /H β by comparison with the corresponding theoretical values for case B recombination (Brocklehurst 1971). The agreement between the reddening-corrected Paschen lines to H α ratios, whenever this measurement was possible, and their theoretical case B recombination values is good.

Reddening-corrected line intensities normalized to H β = 100 are given in Table 2 for each of the H II regions studied. The intensity and equivalent width of the H β line are also given.

None of the regions of our study was observed individually by Smith (1975) who gives line intensity ratios for a combination of regions ('intermediate') which includes CCM10, CCM19 and CCM71. MRS give optical line intensity ratios for four H II regions in M51; for the one we have in common, CCM72, the agreement between our measurements and theirs is very good.

Extinctions derived from Balmer decrements were given by MRS and van der Hulst *et al.* (1988) for some of our

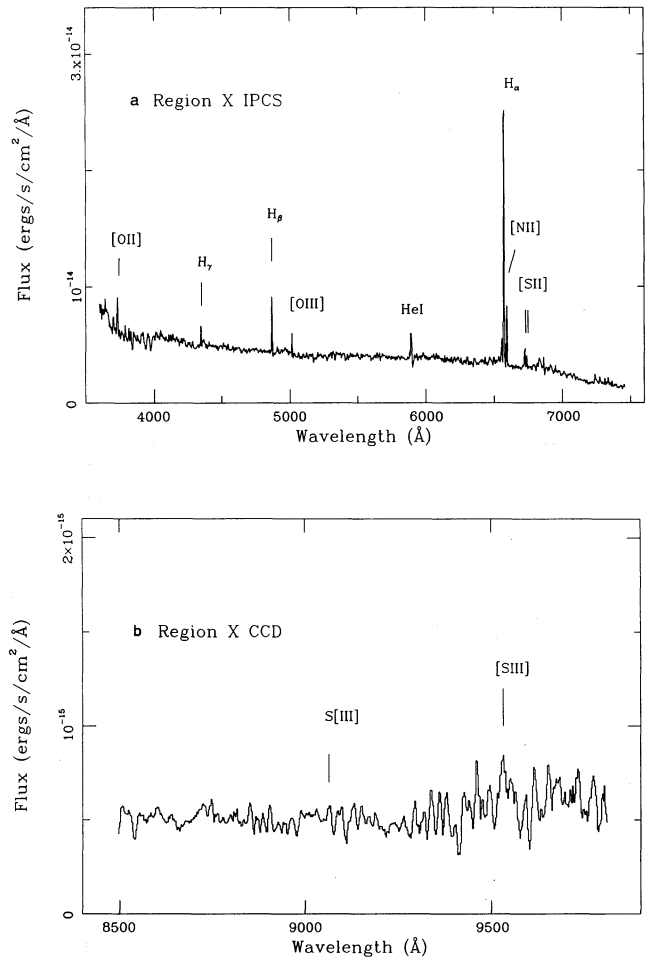


Figure 2. (a) IPCS spectrum of region X. The relevant emission lines are marked. (b) CCD far red spectrum of region X. The nominal positions of the [S III] $\lambda\lambda$ 9069 and 9532 Å are marked.

observed regions and are in good agreement with our determinations. Slightly larger values for CCM71, CCM72 and CCM19 are obtained from radio observations by van der Hulst *et al.* (1988) indicating maybe the presence of clumpy gas around the H II regions.

We have also compared our H α flux values (Table 2) with those given by van der Hulst *et al.* (1988) from H α images for all the observed regions, except X. The agreement is excellent for all the regions except CCM71 for which we measure a flux lower by a factor of about 2.

3.2 Physical conditions in the gas

Electron densities for each observed region were derived from the ratio of the two [S II] lines at $\lambda\lambda 6717, 6731$ Å which implies values of $n_e < 100 \text{ cm}^{-3}$ for all the regions.

Electron temperatures cannot be derived directly from our data since the low excitation of all the regions makes the detection of the [O III] $\lambda 4363$ Å line almost impossible.

Empirical methods exist to estimate average electron temperatures and oxygen abundances (e.g. Pagel *et al.* 1979; Alloin *et al.* 1979). Particularly, the parameter $R_{23} = ([\text{O II}] + [\text{O III}]) / \text{H}\beta$ works as an effective abundance indicator at moderate metallicities where oxygen abundance usually dominates the cooling through the optical lines. However, at metallicities higher than solar, the electron temperatures are very low, IR lines become important and other

elements besides oxygen start to contribute substantially to the cooling complicating this simple picture and making the derivation of oxygen abundance more model dependent. The observed values of the [O II], [O III] and [N II] lines in all cases place the H II regions of M51 at the low-temperature end of the empirical calibration.

The method can be implemented with the introduction of a second indicator, $\eta[\eta = (\text{O}^+/\text{O}^{++})/(\text{S}^+/\text{S}^{++})]$ related to the ionizing spectrum (Vílchez & Pagel 1988). The use of both R_{23} and η would allow the selection of a photo-ionization model reproducing the observed spectrum from an adequate grid (see Vílchez *et al.* 1988). However, since a true calculation of η requires the knowledge of the line temperatures $T_{[\text{O II}]}$ and $T_{[\text{O III}]}$, and equivalent observable parameter can be used: $\eta' = ([\text{O II}]/[\text{O III}])/([\text{S II}]/[\text{S III}])$. At any rate η is not very sensitive to T_e (Vílchez & Pagel 1988) which warrants the equivalence between both parameters η and η' . The values of R_{23} and η' for each of the studied regions are given in Table 3.

4 DETERMINATION OF H II REGION PARAMETERS

4.1 Photo-ionization models

H II regions are a three-parameter family, their emission line spectra being controlled by the shape of the ionizing radia-

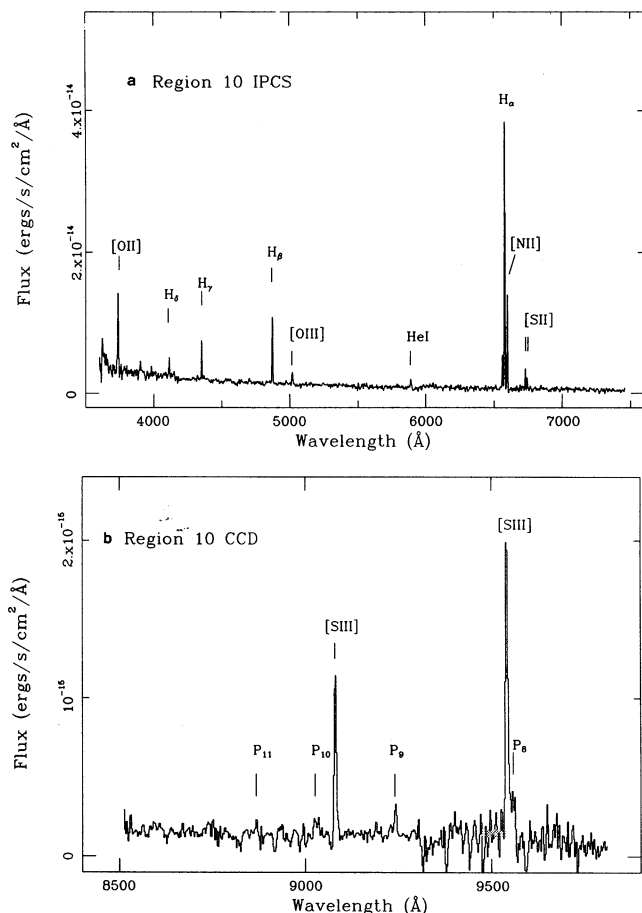


Figure 3. (a) IPCS spectrum and (b) CCD far red spectrum of region CCM10. The relevant emission lines are marked.

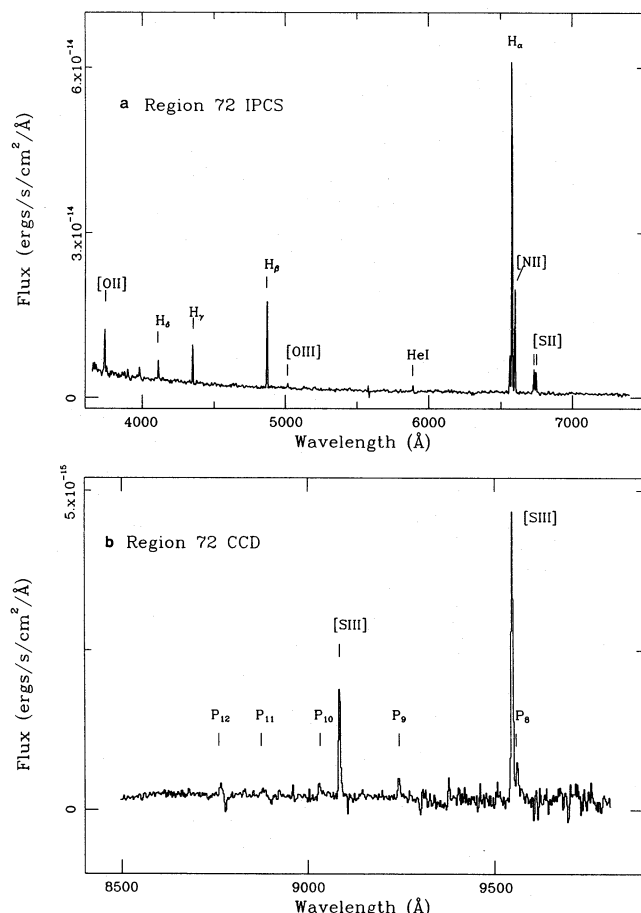
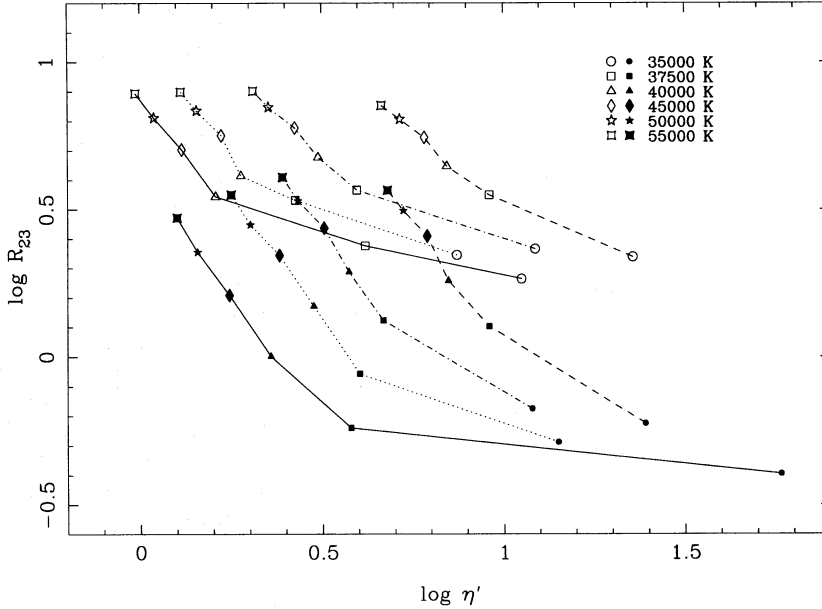


Figure 4. (a) IPCS spectrum and (b) CCD far red spectrum of region CCM72. The relevant emission lines are marked.

Table 3. Derived parameters of the H II regions in M51.

Region	X	CCM 72	CCM 24	CCM 19	CCM 71	CCM 10
$\rho(r)$	0.50	2.22	2.23	2.28	2.44	2.70
$\log R_{23}$	0.17 ± 0.07	-0.16 ± 0.05	0.10 ± 0.06	< -0.33	-0.26 ± 0.14	0.28 ± 0.03
$\log \eta'$	0.11 ± 0.32	1.09 ± 0.05	0.68 ± 0.33	> -0.50	> 0.73	0.75 ± 0.17
$\log u$	-3.71 ± 0.38	-2.80 ± 0.21	-2.98 ± 0.31	-4.09 ± 0.64	-2.92 ± 0.18	-3.08 ± 0.21
$\langle T_{eff} \rangle$	—	36500 K	39000 K	36500 K	35000 K	36500 K
Z/Z_{\odot}	—	2	2	3	2	1.5
ρ = galactocentric distance						
$R_{eff} = 2.60$ arcmin						

**Figure 5.** The abundance parameter R_{23} as a function of η' , for the photo-ionization models described in the text. Open symbols refer to solar abundance models and solid symbols refer to models with twice solar abundances.

tion, the ionization parameter (the ratio of ionizing photon density to particle density) and the chemical composition of the gas. In order to explore the effect of each of the three H II region parameters on R_{23} and η' we have computed simple H II region models using the photo-ionization code CLOUDY whose last version (1990 June) has been kindly made available to us by Gary Ferland.

The models are intended for the analysis of extragalactic H II regions of high metallicity and assume spherical symmetry and uniform density and chemical composition. The nebulae are supposed to be ionized by stars of effective temperatures between 35 000 and 55 000 K whose spectral energy distributions have been taken from the non-local thermal equilibrium (NLTE) atmosphere models of Mihalas (1972);* lower effective temperatures are excluded from consideration by the observed strength of He I. The models have been computed for relatively low values of the ionization parameter ($-4.0 \leq \log u \leq -2.5$) as expected in high metallicity regions (Evans & Dopita 1985; Dopita & Evans 1986; Evans 1986; Vilchez *et al.* 1988), a constant particle density of 10 cm^{-3} and solar and twice solar metal abundances,

where the solar composition has been taken from Stasińska (1990) except for S for which a solar ratio of $S/O = 1.95 \times 10^{-2}$ (Grevesse & Anders 1989) has been used. Effects of internal dust have been neglected; such effects are not expected to change the derived gas phase abundances, ionization parameters or stellar effective temperatures significantly (*cf.* Mathis 1986), but they could affect our estimates of the production rate of Lyman continuum photons and they could be partly responsible for the correlation between chemical composition and ionization parameter that we refer to in Section 5 below.

Similar photo-ionization models have recently been computed by Stasińska (1990). However, a direct comparison between both sets of models is difficult since the chosen ionization parameters do not overlap, Stasińska's being too large for high metallicity objects. The CLOUDY photo-ionization code includes reasonable estimates of the dielectronic recombination coefficients for sulphur. Although these are not yet accurately known, their inclusion is expected to enable the S^{++}/S^+ ratio to be predicted to an accuracy of approximately 25 per cent, which is comparable to the accuracy with which it can be measured observationally.

Fig. 5 shows R_{23} versus η' for the models computed. Open symbols refer to solar abundance models while solid ones

*The reasons why we prefer Mihalas (1972) models to others currently available have been given by Vilchez & Pagel (1988).

refer to models with twice the solar abundance. Solid, dotted, dash-dotted and dashed lines connect models with $\log u = -2.5, -3.0, -3.5$ and -4.0 respectively. It can be seen from the figure that the parameter η' reflects mainly the shape of the ionizing continuum and therefore depends strongly on the effective temperature of the ionizing stars. It also depends on ionization parameter, but it is almost independent of global metal abundance. The R_{23} parameter, in turn, depends mainly on the chemical composition of the gas and the effective temperature of the ionizing stars, being almost independent of ionization parameter.

Therefore, once the ionization parameter is known, the position of a given region in the diagram allows the simultaneous determination of the effective temperature of the ionizing stars and the overall metallicity of the gas. Of course, both R_{23} and η' depend to some extent on element ratios, mainly S/O and N/O. This effect can be seen in Fig. 6 where we show models with $\log u = -3.0$ and with solar abundances apart from having different S/O and N/O ratios. An increase of S/O and N/O over the solar ratio makes the nebula cooler with a corresponding decrease in R_{23} and the opposite happens when the S/O ratio is lowered below its solar value. It can be seen that a solar model with an overabundance of nitrogen and an underabundance of sulphur mimics the behaviour of the solar composition model in the R_{23} versus η' diagram. These relative abundances can only be determined by detailed model fitting to the emission lines of the individual H II regions.

The ionization parameter can, in principle, be deduced from the sulphur ionic ratio S^+/S^{++} (Mathis 1985), but can equally be derived from the line ratio $[S II] (6717+6731)/[S III] (9069+9532)$. Fig. 7 shows the relation between the logarithm of this ratio and $\log u$ for the computed models. Again open and solid circles refer to solar and twice solar abundance models respectively. Effective temperatures are as labelled, in units of 1000 K. A good relation exists in-

dependently of metallicity and effective temperature, that can be fitted by the regression line

$$\log u = (-1.684 \pm 0.076) \log([S II]/[S III]) - (2.986 \pm 0.027)$$

Following this relation we have derived ionization parameters for each of the H II regions of M51 and they are listed in Table 3. All of them are low, ranging from -2.98 for CCM24 to -4.10 for CCM19. The errors quoted include the observational error in the $[S II]/[S III]$ ratio and the error in the regression line.

4.2 Abundance determinations

Fig. 8 shows the position of the observed H II regions in the $\log R_{23}$ versus $\log \eta'$ plane represented by their corresponding error boxes. For regions CCM19 and CCM71 the data give an upper limit to $\log R_{23}$ and a lower limit to $\log \eta'$ respectively. According to these positions we have made a first estimation of the effective temperature of the ionizing radiation, T_{eff} , and the overall metallicity of each region and they are listed in Table 3. No satisfactory combination of ionization parameter and metallicity can be found for region X. This region, being so close to the active nucleus of M51, is probably contaminated by its ionizing continuum.

With these first estimations we proceeded to individual model fitting. In Table 4 we list the emission line ratios corresponding to the best fitting model for each of the observed H II regions together with their observed values and the relevant parameters of the models. The points corresponding to these models are plotted in Fig. 8 as stars. Table 5 gives the corresponding abundances and temperatures derived for each of the regions.

5 DISCUSSION

Having determined the functional parameters: T_{eff} , $\log u$ and Z for each of the observed H II regions, we are now in a position to study their physical properties.

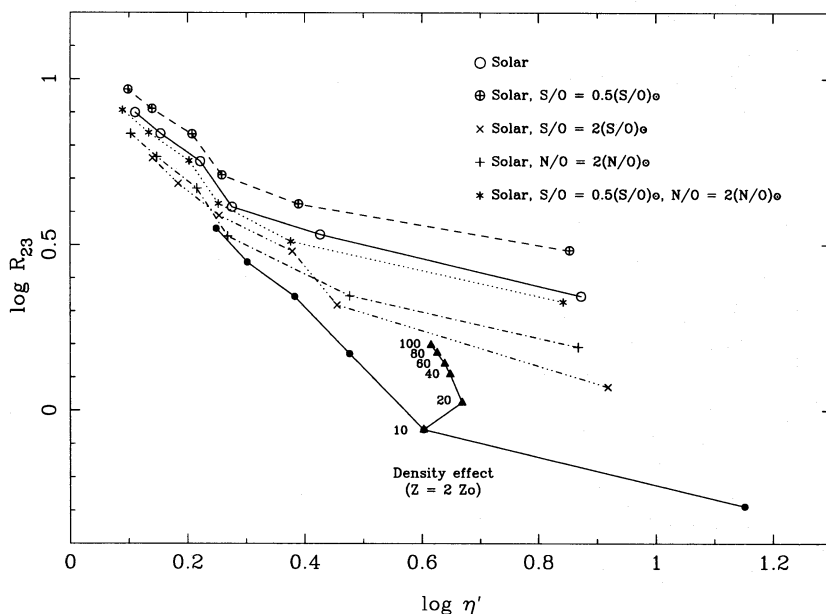


Figure 6. Same as Fig. 5 but showing the effect of changing the nitrogen and sulphur abundances relative to oxygen on solar abundance models with $\log u = -3.0$. The effect of increasing the particle density up to 100 cm^{-3} on models with twice solar abundances is also shown.

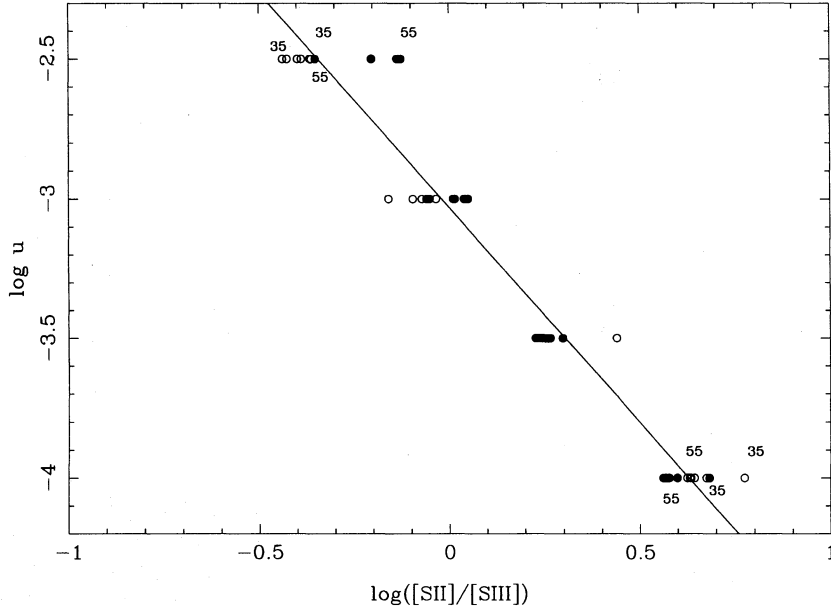


Figure 7. Relation between ionization parameter and $[S II]/[S III]$ as deduced from the photo-ionization models described in the text. Open and solid symbols refer to solar and twice solar models respectively.

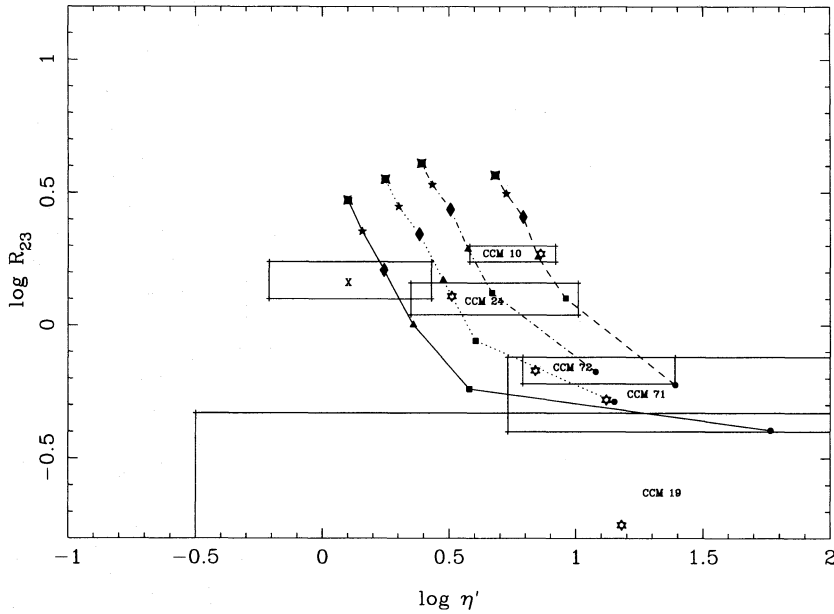


Figure 8. Position of the observed H II regions in M51 on the R_{23} versus η' diagram. Symbols are as in Fig. 5. Error boxes are shown. The best fitting model for each region is plotted as a star. No model has been fitted for region X.

The fact that our H α fluxes are in very good agreement with those given by van der Hulst *et al.* (1988) seems to indicate that our spectra are representative of the whole regions and therefore our spectrophotometry can be used to determine the total number of ionizing photons (N_{Ly}) required to sustain them (see for example Osterbrock 1974). These values have been computed for an assumed distance of 9.6 Mpc for M51 (Sandage & Tammann 1974) and are listed in Table 6. They are comparable to those of other H II

regions like NGC 604 in M33 and 30 Dor in the LMC. The values of the observed H β fluxes, when combined with the low ionization parameters found and the observed sizes of the regions (van der Hulst *et al.* 1988) yield the particle densities, n_H , filling factors, f , and masses of ionized hydrogen, $M_{H II}$, listed in Table 6. (These have been derived using the formulae listed at the foot of that table, which can easily be verified by the reader.) The derived values of n_H are close to the assumed one of 10 cm^{-3} except for CCM19

Table 4. Photo-ionization models for the observed H II regions.

Region	CCM 72		CCM 24		CCM 19		CCM 71	
	Model	Observed	Model	Observed	Model	Observed	Model	Observed
T_{eff} (K)	36000	—	39000	—	36500	—	35000	—
$\log u$	-3.10	-2.80 ± 0.21	-3.00	-2.98 ± 0.31	-4.00	-4.09 ± 0.64	-3.00	-2.92 ± 0.18
Z/Z_{\odot}	2	—	2	—	3	—	2	—
n_H	10	—	10	—	10	—	10	—
$\log[\text{OII}]/\text{H}\beta$	-0.23	-0.21 ± 0.04	-0.01	0.01 ± 0.02	-0.76	< -0.55	-0.32	-0.34 ± 0.10
$\log[\text{OIII}]/\text{H}\beta$	-1.07	-1.15 ± 0.15	-0.49	-0.64 ± 0.2	-2.47	< -0.74	-1.38	< -1.0
$\log[\text{SII}]/\text{H}\beta$	-0.34	-0.28 ± 0.06	-0.36	-0.38 ± 0.03	-0.44	-0.41 ± 0.06	-0.43	-0.46 ± 0.06
$\log[\text{SIII}]/\text{H}\beta$	-0.34	-0.28 ± 0.06	-0.33	-0.35 ± 0.15	-0.97	-1.1 ± 0.3	-0.37	-0.39 ± 0.04
$\log[\text{NII}]/\text{H}\beta$	0.08	0.09 ± 0.01	0.16	0.16 ± 0.04	0.00	0.02 ± 0.04	0.03	0.06 ± 0.04
$\log R_{23}$	-0.17	-0.16 ± 0.05	0.11	0.10 ± 0.06	-0.75	< -0.33	-0.28	-0.26 ± 0.13
$\log \eta'$	0.84	1.09 ± 0.30	0.51	0.68 ± 0.33	1.18	> -0.50	1.12	> 0.73

Table 5. Line temperatures and abundances for H II regions of M51 deduced from models.

Region	CCM 72	CCM 24	CCM 19	CCM 71	CCM 10
$t([\text{OIII}])$	0.41	0.40	0.37	0.39	0.54
$t([\text{OII}])$	0.48	0.51	0.39	0.46	0.60
$12 + \log(\text{O}/\text{H})$	9.22	9.22	9.40	9.22	9.11
$\log(\text{N}/\text{O})$	-0.78	-0.75	-0.63	-0.78	-0.93
$\log(\text{S}/\text{O})$	-1.80	-1.88	-1.90	-1.80	-2.05

Table 6. Physical characteristics of the H II regions in M51.

Region	CCM 72	CCM 24	CCM 19	CCM 71	CCM 10
$\log N_{\text{Ly}}$	51.70	51.14	51.00	51.27	51.51
$\log u$	-3.10	-3.00	-4.00	-3.00	-3.05
$\phi(\text{arcsec})^*$	11.3	12.0	10.5	12.8	12.0
n_H^*	26	5	47	6	13
f^*	0.014	0.06	0.001	0.05	0.02
$M_{\text{HII}}^* (10^5 M_{\odot})$	6.3	9.0	0.7	10.2	8.0
$M_{\text{min}} (10^4 M_{\odot})$	5.5	1.5	1.1	2.0	3.5

*Angular diameter ϕ from van der Hulst *et al.* (1988).

$$f = 0.03 \left(\frac{10^{-13} \text{ erg cm}^{-2} \text{ s}^{-1}}{I(\text{H}\beta)} \right) \left(\frac{u}{10^{-3}} \right)^2 \left(\frac{\phi}{10 \text{ arcsec}} \right) \times \left(\frac{9.6 \text{ Mpc}}{D} \right)$$

$$\frac{n_H}{10 \text{ cm}^{-3}} = \left(\frac{I(\text{H}\beta)}{10^{-13} \text{ erg cm}^{-2} \text{ s}^{-1}} \right) \left(\frac{10^{-3}}{u} \right) \left(\frac{10 \text{ arcsec}}{\phi} \right)^2$$

$$\frac{M_{\text{HII}}}{M_{\odot}} = 6.2 \times 10^5 \left(\frac{u}{10^{-3}} \right) \left(\frac{\phi}{10 \text{ arcsec}} \right)^2 \left(\frac{D}{9.6 \text{ Mpc}} \right)^2$$

where it seems somewhat higher, but this is also the region for which it is most uncertain through the uncertainty in u (see Table 3). Filling factors are small, between 0.001 and 0.06, values not uncommon in giant H II regions. The corresponding masses of ionized gas, M_{HII} , are accordingly smaller than those given by van der Hulst *et al.* (1988).

The derived number of ionizing photons, N_{Ly} , indicates that our H II regions are ionized by a cluster of stars. The

functional parameter, T_{eff} , should then be taken as the effective temperature of the stars and dominate the ionization, and is in the range from 35 000 K to 39 000 K.

For a given star cluster, we can obtain the number of ionizing stars from the total number of ionizing photons per unit mass as

$$N_{\text{Ly}} = \sum_{T,L} N(T,L) N_{\text{Ly}}(T,L),$$

where $N(T,L)$ denotes the number of stars, per unit mass of the cluster, of each effective temperature and luminosity and $N_{\text{Ly}}(T,L)$ their corresponding number of ionizing photons. For a Zero Age Main Sequence (ZAMS) N_{Ly} can be calculated for an assumed (IMF) in a straightforward manner. For a power-law IMF with lower and upper initial mass function mass limits of 1 and $120 M_{\odot}$ respectively, and slope $-\alpha = -2.35$ (Salpeter) and the values of ionizing photon numbers of main-sequence stars, $N_{\text{Ly}}(T, L_{\text{MS}})$, given by Panagia (1973), we obtain a value of N_{Ly} of $9.14 \times 10^{46} \text{ s}^{-1} M_{\odot}^{-1}$. Higher values of α , as suggested by recent observations (see Scalo 1986), as well as lower upper mass limits would reduce N_{Ly} as also would any subsequent evolution of the cluster. Therefore the calculated number allows us to set lower limits to the masses of the ionizing clusters (M_{min}) which are also listed in Table 6. These masses range from 1 to $5.5 \times 10^4 M_{\odot}$, about one hundredth of the mass of ionized hydrogen.

The relatively low values of T_{eff} indicate that we are probably dealing with evolved star clusters. If the deduced values of T_{eff} can be taken as the effective temperatures of the stars at the turnoff, the implied ages for the observed H II regions, according to recent models of stellar evolution (Maeder & Meynet 1987; Maeder 1991), are between 2 and 5 Myr. However, ionizing clusters of these characteristics would produce $\text{H}\beta$ equivalent widths much larger than the ones observed (e.g. Dottori 1981), pointing to the presence of an underlying older stellar population which contributes substantially to the continuum while producing negligible emission. This would be the case if these H II regions are formed by subclusters of stars of different ages. The older ones would provide most of the continuum at $\text{H}\beta$ while the bulk of the emission would come from the youngest ones. Spatially resolved observations of other giant H II regions like NGC 604 in M33 (Díaz *et al.* 1987) and NGC 5471 in M101 (Skillman 1985) tend to support this picture.

The oxygen abundances found in this investigation are all higher than solar. The ionization parameters for each of the regions are also low conforming to the relation between ionization parameter and metallicity suggested by Evans & Dopita (1985), Dopita & Evans (1986), Evans (1986) and Vílchez *et al.* (1987).

These abundances have been calculated from photo-ionization models assuming an electron density of 10 cm^{-3} . The effect of increasing the density to 30, 60, 80 and 100 cm^{-3} can be seen in Fig. 6 for the model of $T_{\text{eff}} = 37\,000 \text{ K}$, $\log u = -3.0$ and twice solar metallicity. At these effective temperatures, a density increase leads to a strengthening of the lines thus moving the model points up in the diagram. Abundances calculated using models with densities higher than 10 cm^{-3} would yield abundances higher than the ones found by us. For example, for region CCM10 the chosen model with $n_{\text{H}} = 10 \text{ cm}^{-3}$ with $Z/Z_{\odot} = 1.5$ a similar model with $n_{\text{H}} = 30 \text{ cm}^{-3}$ and $Z/Z_{\odot} = 2.0$ give equally good fits to the observations. The relative abundances of N/O and S/O remain the same and do not seem to depend on particle density. The choice of a low density seems to represent then a conservative approach and does not alter our deductions about relative abundances.

All of the observed H II regions up to a galactocentric distance of 7.56 kpc (assuming a distance $D = 9.60 \text{ Mpc}$ for M51; Sandage & Tammann 1974) show overall metallicities higher than solar which probably makes M51 the spiral with the highest abundances known. CCM71 and CCM72 at galactocentric distances of 6.83 and 6.24 kpc respectively to the south-west show the same abundances, as expected given the close location of these two regions in the galaxy (see Plate 1). However, the regions to the north-east (the direction of the companion galaxy NGC 5195): CCM10, CCM19 and CCM24 show different abundances, between 1.5 and 3 times solar, the lowest abundance corresponding to the region with the largest galactocentric distance. Unfortunately the small range of distances covered by our observations precludes the determination of an abundance gradient, but an idea of this can be obtained by considering the $[\text{O III}]/\text{H}\beta$ ratios

measured by us, by Smith (1975), by McCall, Rybski & Shields (1985) and by Zaritsky, Elston & Hill (1990), which are shown in Fig. 9 as a function of galactocentric distance, R , in units of the effective radius, R_{eff} (from McCall 1982). Reference to the rough calibration of $[\text{O III}]/\text{H}\beta$ against oxygen abundance given by Edmunds & Pagel (1984) shows a reduction of almost an order of magnitude over 4 effective radii, which is within the scatter displayed by other Sb and Sc spirals plotted (together with preliminary estimates for M51 itself) in that paper. According to our new analysis, the reduction is more accurately estimated to be a factor of 5 for M51, and the same factor may well apply also to the other early-type spirals.

Our detailed fitting points to S/O and N/O ratios different from solar for these high-metallicity regions. The ratio of N/O is different from solar in all regions but CCM10, and seems to increase with metallicity as expected if the secondary production of nitrogen increases with age and/or metallicity. The ratio of S/O is lower than solar in all the observed regions. It is difficult to know if these overabundances are real or are just an artefact of the models caused by poor knowledge of atomic parameters, particularly in the case of sulphur. However, the same method applied here to the H II regions of M51 when applied to S5 (data from Shields & Searle 1978; Torres-Peimbert, Peimbert & Fierro 1989; Díaz *et al.* 1990), one of the best studied regions of M101, yields abundances which are solar with no deviations from the solar ratios.

The existence of an anticorrelation between S/O and O/H has been claimed by several authors for the Galaxy (Talent & Dufour 1979; Shaver *et al.* 1983), M101 (Evans 1986) and M33 (Vílchez *et al.* 1988) and later questioned by Garnett (1989) who finds no evidence for an increase in S/O in regions with low O/H. Our data seem to support the conclusion that, at least, there is a decrease of S/O in regions with high O/H. Fig. 10 shows $\log(\text{S/O})$ versus $12 + \log(\text{O/H})$ for regions of relatively high metallicity ($12 + \log(\text{O/H}) \geq 8.3$). The data have been taken from Shaver *et al.* (1983) for the Galaxy, Vílchez *et al.* (1988) for M33, Díaz *et al.*

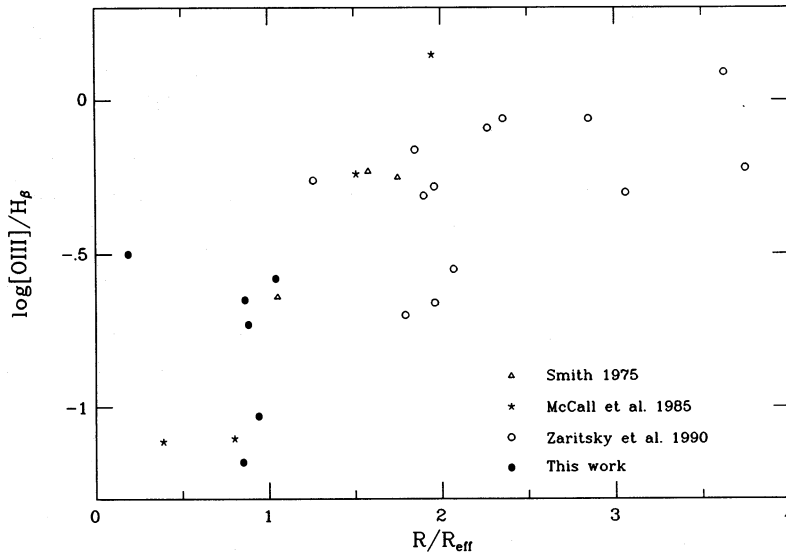


Figure 9. The $[\text{O III}]/\text{H}\beta$ ratio as a function of galactocentric distance, normalized to the effective radius of the galaxy, for H II regions in M51. References for the data are given in the text.

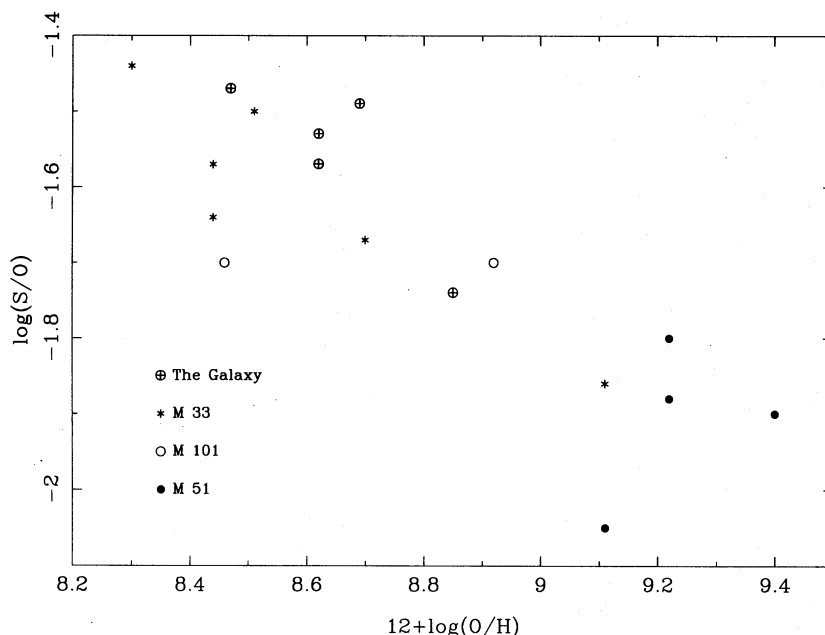


Figure 10. The S/O ratio as a function of oxygen content for H II regions in the Galaxy, M33, M101 and M51, with $12 + \log(\text{O}/\text{H}) > 8.3$. References for the data are given in the text.

al. (1990) for M101 and this work for M51. Data on CC93 in M33 and S5 in M101 have been re-analysed according to the method outlined in this paper. In these regions sulphur is mainly in the form of S^+ and S^{++} and both [S II] and [S III] lines have been observed in all cases. Only a few regions: NGC 604, NGC 599 and NGC 5461 require a small correction for the presence of S^{3+} that we have deduced from Garnett (1989). For these high-metallicity regions there is a clear relation between S/O and O/H in the sense of a decreasing S/O ratio in regions of high oxygen content.

Theoretically, sulphur comes from hydrostatic and explosive burning of O and Si and stars with masses greater than $10 M_{\odot}$ are the most likely candidates for its production. The S/O ratio produced is greater for stars with masses in the range $12\text{--}20 M_{\odot}$; then, in principle, variations in the IMF for massive stars could produce variations in the S/O ratio. Garnett (1989). For these high-metallicity regions there is a trend models with varying IMF slopes and upper mass limit according to metallicity following prescriptions by Campbell (1988) and Terlevich (1985) resulting in positive trends of S/O with O/H contrary to what seems to be observed. On the other hand, Matteucci & François (1989) are able to generate a small positive gradient of S/O in models of the galactic disc.

More studies of high-metallicity H II regions are obviously needed in order to assess the reality of any trend of S/O with oxygen abundance.

6 CONCLUSIONS

We have studied in detail six giant low-excitation H II regions in the spiral galaxy M51 using spectrophotometric observations between 3500 and 9700 Å, and theoretical photo-ionization models, as an extension of our previous work to the high-metallicity domain.

For each region, except X whose spectrum is probably contaminated by radiation from the LINER nucleus, we have been able to determine the ionization parameter, the effective temperature of the cluster stars dominating the ionization and the metallicity. All regions have metallicities higher than solar and both ionization parameter and effective temperature are low, extending previously found trends between metallicity and ionization parameter and radiation hardness.

The H II regions in M51 are large ($R \approx 250$ pc), diffuse ($n_{\text{H}} \leq 100 \text{ cm}^{-3}$) and have small filling factors. The mass of ionized hydrogen is of the order of $10^6 M_{\odot}$ and the minimum mass of the ionizing star clusters is of the order of $10^4 M_{\odot}$. Some contribution from older clusters is suggested in view of the small H β equivalent widths observed.

S/O ratios are lower than solar in all the studied regions. If this effect is not due to model artefacts it implies that the S/O ratio is lower in regions with high metal content, something that should be explained by stellar nucleosynthesis theory and chemical evolution models. N/O ratios are also different from solar in all but one of the regions, increasing with metallicity as expected if part of the nitrogen is of secondary origin.

The combination of spectrophotometric observations over a wide spectral range, including the nebular [S III] lines, and adequate photo-ionization models proves to be a very powerful tool for determining reliable abundances and physical conditions in low-excitation regions that can lead to a better understanding of their properties and evolution.

ACKNOWLEDGMENTS

The INT is operated on the island of La Palma by the RGO at the Observatorio del Roque de los Muchachos of the Instituto de Astrofísica de Canarias. We thank both committees PATT and CAT for awarding observing time and acknow-

ledge fruitful discussions with Gary Ferland, Don Garnett, Evan Skillman and Grazyna Stasińska.

Partial financial support from the Spanish CAICYT under project PB86-0292-C04-03 is acknowledged.

REFERENCES

- Alloin, D., Collin-Souffrin, S., Joly, M. & Vigroux, L., 1979. *Astr. Astrophys.*, **78**, 200.
- Brocklehurst, M., 1971. *Mon. Not. R. astr. Soc.*, **153**, 471.
- Campbell, A. W., 1988. *Astrophys. J.*, **335**, 644.
- Carranza, G., Crillon, R. & Monnet, G., 1969. *Astr. Astrophys.*, **1**, 479 (CCM).
- Díaz, A. I., 1989. In: *Evolutionary Phenomena in Galaxies*, eds Beckman, J. E. & Pagel, B. E. J., Cambridge University Press, Cambridge.
- Díaz, A. I., Terlevich, E., Pagel, B. E. J., Vilchez, J. M. & Edmunds, M. G., 1987. *Mon. Not. R. astr. Soc.*, **226**, 19.
- Díaz, A. I., Pagel, B. E. J. & Wilson, I. R. G., 1985. *Mon. Not. R. astr. Soc.*, **212**, 737.
- Díaz, A. I., Terlevich, E., Pagel, B. E. J., Vilchez, J. M. & Edmunds, M. G., 1987. *Mon. Not. R. astr. Soc.*, **226**, 19.
- Díaz, A. I., Terlevich, E., Pagel, B. E. J., Vilchez, J. M. & Edmunds, M. G., 1990. In: *Dynamical and Chemical Evolution of Galaxies*, eds Franco, J. J., Matteucci, F. & Ferrini, F.
- Dopita, M. A. & Evans, I. N., 1986. *Astrophys. J.*, **307**, 431.
- Dottori, H., 1981. *Astrophys. Sp. Sci.*, **80**, 267.
- Edmunds, M. G. & Pagel, B. E. J., 1984. *Mon. Not. R. astr. Soc.*, **211**, 107.
- Evans, I. N., 1986. *Astrophys. J.*, **309**, 544.
- Evans, I. N. & Dopita, M. A., 1985. *Astrophys. J. Suppl.*, **58**, 125.
- Ferland, G., 1990. *OSU Internal Report 90-02*.
- Garnett, D. R., 1989. *Astrophys. J.*, **345**, 282.
- Grevesse, N. & Anders, E., 1989. In: *Cosmic Abundances of Matter*, AIP Conf. Proc. No. 183, ed. Waddington, C. J., New York.
- McCall, M. L., 1982. *PhD thesis*, University of Texas, Austin, USA.
- McCall, M. L., Rybski, P. M. & Shields, G. A., 1985. *Astrophys. J. Suppl.*, **57**, 1(MRS).
- Maeder, A., 1991. *Astr. Astrophys. Suppl.*, in press.
- Maeder, A. & Meynet, G., 1987. *Astr. Astrophys.*, **182**, 243.
- Mathis, J. S., 1982. *Astrophys. J.*, **261**, 195.
- Mathis, J. S., 1985. *Astrophys. J.*, **291**, 247.
- Mathis, J. S., 1986. *Publs astr. Soc. Pacif.*, **98**, 995.
- Matteucci, F. & François, P., 1989. *Mon. Not. R. astr. Soc.*, **239**, 885.
- Mihalas, D., 1972. *Non-LTE Model Atmospheres for B and O Stars*, NCARTN/STR-76.
- Osterbrock, D. E., 1974. *Astrophysics of Gaseous Nebulae*, Freeman, San Francisco.
- Pagel, B. E. J., Edmunds, M. G., Blackwell, D. E., Chun, M. S. & Smith, G., 1979. *Mon. Not. R. astr. Soc.*, **189**, 95.
- Panagia, N., 1973. *Astr. J.*, **78**, 929.
- Rose, J. A. & Searle, L., 1982. *Astrophys. J.*, **253**, 556.
- Rose, J. A. & Cecil, G., 1983. *Astrophys. J.*, **266**, 531.
- Sandage, A. & Tammann, G. A., 1974. *Astrophys. J.*, **194**, 559.
- Scalo, J. M., 1986. *Fund. Cosmic Phys.*, **11**, 1.
- Shaver, P. A., McGee, R. X., Danks, A. C. & Pottasch, S. R., 1983. *Mon. Not. R. astr. Soc.*, **204**, 53.
- Shields, G. A. & Searle, L., 1978. *Astrophys. J.*, **222**, 821.
- Skillman, E. D., 1985. *Astrophys. J.*, **290**, 449.
- Smith, H., 1975. *Astrophys. J.*, **199**, 591.
- Stasińska, G., 1982. *Astr. Astrophys. Suppl.*, **48**, 299.
- Stasińska, G., 1990. *Astr. Astrophys. Suppl.*, **83**, 501.
- Talent, D. L. & Dufour, R., 1979. *Astrophys. J.*, **233**, 888.
- Terlevich, R., 1985. In: *Star Forming Dwarf Galaxies and Related Objects*, p. 395, eds Kunth, D., Thuan, T. X. & Thanh Van, J. T., Editions Frontières, Gif Sur Yvette, France.
- Torres-Peimbert, S., Peimbert, M. & Fierro, J., 1989. *Astrophys. J.*, **345**, 186.
- van der Hulst, J. M., Kennicutt, R. C., Crane, P. C. & Rots, A. H., 1988. *Astr. Astrophys.*, **195**, 38.
- Vilchez, J. M. & Pagel, B. E. J., 1988. *Mon. Not. R. astr. Soc.*, **231**, 257.
- Vilchez, J. M., Pagel, B. E. J., Díaz, A. I., Terlevich, E. & Edmunds, M. G., 1988. *Mon. Not. R. astr. Soc.*, **235**, 633.
- Zaritsky, D., Elston, R. & Hill, J. M., 1990. *Astr. J.*, **99**, 1108.